Assessing Mesoscopic Organization in Copolymer-Templated Silica Hybrid Films *via* Solid-State Nuclear Magnetic Resonance

Abraham Chemtob,[1,2]* *Mathilde Sibeaud,*[1,2,3] *Céline Croutxé-Barghorn,*[2,3] *Cyril Vaulot,*[1,2] *Séverinne Rigolet,*[1,2] *Laure Michelin,*[1,2] *Loïc Vidal,*[1,2] *Bénédicte Lebeau*[1,2]

[1] Institut de Science des Matériaux de Mulhouse, IS2M UMR 7361 CNRS, Université de Haute-Alsace, France

[2] Université de Strasbourg, 4 rue Blaise Pascal, 67081 Strasbourg, France

[3] Laboratory of Macromolecular Photochemistry and Engineering, University of Haute-Alsace, ENSCMu, 3 bis rue Alfred Werner, 68093 Mulhouse Cedex, France

* Corresponding author: E-mail: abraham.chemtob@uha.fr; Tel: +33 3 8960 8834

Abstract

In the context of increasing use of nanostructured materials, finding innovative characterization methods able to assess precisely the level of ordering is essential. To this end, a range of model organic-inorganic copolymer-silica films is synthesized using poly(ethylene oxide)-*b*-poly(propylene oxide)-*b*-poly(ethylene oxide) amphiphilic triblock copolymer as supramolecular template. Upon increasing copolymer concentration (10 – 100 wt%), the order can be gradually enhanced from short-range to long-range as proved by conventional techniques such as X-ray diffraction and electron microscopy. To evaluate the level of mesoscopic organization, the same series of samples is also analyzed by solid-state nuclear magnetic resonance (NMR) spectroscopy. The disorder-to-order transition is probed by ^{1}H and ^{13}C magic angle spinning NMR spectra through the increase in chemical environment uniformity and chain mobility respectively, which both result from the self-assembly mechanism. ^{1}H NMR relaxation measurements (T_2) using low-field NMR spectroscopy are instrumental to identify the threshold template concentration where ordering takes place.

Keywords: Hybrid materials; Amphiphilic block copolymer; Mesoporous; Mesostructuration; Self-assembly; Poloxamer; Sol-gel; 1H Nuclear relaxometry

1. Introduction

The discovery of surfactant-templated silica mesophases in 1992 has marked the start of a wave of nanostructured materials [1]. Periodically organized mesoporous materials are the best known because they are uniquely characterized by high specific surface areas (500 - 1000 m^2 g^{-1}), uniform mesopores (2 - 20 nm), and a highly ordered structure leading to a well-defined geometric pore arrangement. The most recent developments currently cover energy conversion [2] and storage devices [3]. Surfactant self-assembly using amphiphilic copolymer has also served to create mesostructured polymer-inorganic hybrid materials used as electrolyte membranes [4], mechanically resistant coatings [5] or nanophotonics devices [6]. For these two classes of nanostructured materials relying on liquid crystal templating, the precise structural characterization is critical, because the final material properties depend on the mesoscopic structure [7].

As more and more nanostructured materials are now introduced in the market, there is the challenge of finding non-destructive and reliable methods to characterize the mesoscopic structure [8,9]. Currently, two main physico-chemical techniques are used to probe the structure of mesostructured materials [10]: X–ray diffraction (XRD) and transmission electron microscopy (TEM). While these techniques have been extremely valuable for laboratory investigations, they are less adequate for industrial production controls because they are time-consuming, expensive and still largely subjective, i.e. based on the judgment of a trained investigator. Additionally, it is also common that several characterization techniques are used in conjunction with one another to get unequivocal structural features. Under these conditions, there is the need of other characterization means able to ensure that the mesostructure's level of ordering is uniform, high and does not fall below established standards. In this domain, very few technical developpments have been pursued, mainly for mesoporous materials,

including ellipsometric porositimetry [11], thermoporometry [12], positron annihilation spectroscopy [13], or fluorescent technique [14].

The objective of this work is to investigate the potential of solid-state nuclear magnetic resonance (NMR) analysis for the characterization of mesostructured polymer-silica hybrid films prepared by sol-gel chemistry with amphiphilic block copolymer template acting as template. Solid-state NMR spectroscopy has been already employed to characterize this class of materials, but mostly to determine the coordination status of silicon atoms [15], and in very few cases to examine the mesoscopic structure [16–20]. As sketched in **Scheme 1**, when a highly ordered mesoscopic order is achieved in polymer-silica hybrid (right image), the amphiphilic block copolymer is characterized by a spatial separation at the nanometer scale of the hydrophilic and hydrophobic segments. This phase segregation results in a better *chemical environment uniformity* but also a higher *mobility* of the hydrophobic block because the nonpolar interior of the mesophase provides increased freedom compared to the densely cross-linked silica matrix. Conversely, the amorphous structure (left image) shows two intimately mixed block segments, remaining in close interfacial contact with the rigid silica network. In this second case, the hydrophobic block has a range of possible chemical environments and is more motionally restricted (provided that a dense silica matrix is formed).

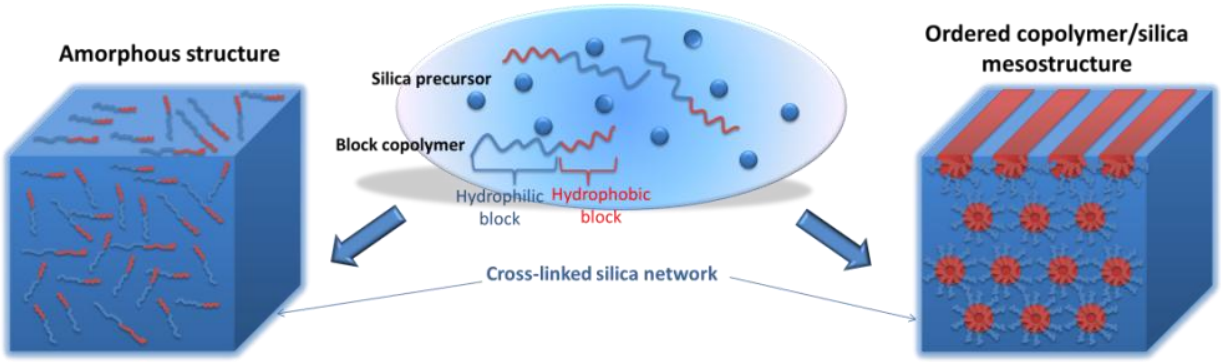

Scheme 1. A phase segregation of the hydrophobic segment of the amphiphilic block copolymer accompanies the sol-gel induced self-assembly process, leading to a well-ordered hexagonal array of cylinders (right). When self-organization fails, an amorphous composite is formed showing an ideal homogenous mixture of individual chains or aggregates of block copolymer occluded within the silica matrix (left).

In this report, a range of copolymer-silica hybrid films has been prepared using as template the poloxamer poly(ethylene oxide)$_{20}$-poly(propylene oxide)$_{70}$-poly(ethylene oxide)$_{20}$ (PEO_{20}-*b*-PPO_{70}-*b*-PEO_{20}). This poloxamer is also known by its trade name Pluronic 123 or P123 [21]. The degree of mesoscopic organization has been modulated by changing the concentration in amphiphilic copolymer. Firstly, the hybrid films' mesostructural ordering was analyzed by two conventional methods: XRD and TEM. As a more original characterization technique, solid-state NMR spectroscopy was used to probe the disorder-to-order transition through its well established sensitivity to *chemical uniformity* for ^{13}C NMR and *chain mobility* for ^{1}H NMR, which should be both enhanced upon increasing mesoscopic order [16]. Starting from the same series of samples, ^{1}H T_2 NMR relaxation measurements [22] were also performed to exploit the increased *mobility* of PEO-*b*-PPO-*b*-PEO chains when mesoscopic organization of silica/copolymer hybrid arises.

2. Experimental Section

2.1 Materials

Pluronic 123 (P123) and diphenyl iodonium hexafluorophosphate (photoacid generator, Φ_2I^+ PF_6^-) were purchased from Sigma Aldrich. Poly(dimethoxysiloxane) (PDMOS) is an oligomeric methoxy precursor provided by ABCR (with a proportion of $Q_0/Q_1/Q_2/Q_3$ species: 4.5/26.5/48.5/20.5 % as determined by liquid-state ^{29}Si NMR spectrum). After washing with acetone, polished silicon wafers (Siltronix) and glass substrate (Brot, 10 × 10 cm) were used as substrates for the preparation of the P123-silica hybrid films.

2.2 UV-driven synthesis of PEO_{20}-*b*-PPO_{70}-*b*-PEO_{20}-silica hybrid films

A homogeneous and stable solution containing PDMOS, P123, photoacid generator (Φ_2I^+ PF_6^-) and acetone was prepared. A total of seven formulations were prepared upon

varying *x* the weight fraction in P123 with respect to silica precursor from 0.1 to 1: PDMOS/P123/$\Phi_2I^+PF_6^-$/acetone = 1/*x*/0.06/1 (*x* = 0.1 – 1). Samples were prepared via a light induced self-assembly protocol [21,23]. The typical procedure begins by casting the photolatent solution using a 4 µm bare coater on a glass or silicon wafer. The as-desposited samples were placed into an environmental chamber (Memmert HCP 108 hygrometric chamber) where temperature (T) and relative humitidy (RH) were controlled throughout the experiment: T = 30 °C and RH = 60 %. To ensure the homogeneous irradiation of the P123/PDMOS liquid films, two fluorescent UV bulbs UV 6 (36 W, Philips, Waldmann UV236 system) were placed inside the chamber above the samples (distance = 6 cm). Their emission wavelength spans from 280 to 380 nm, with an total irradiance of 3 mW cm^{-2} measured at the surface of the sample. The films were irradiated continuously for 30 min. UV irradiation causes the photoacid generator photodecomposition and the subsequent release of superacids ($H^+PF_6^-$). These photoacids were proved to catalyze the hydrolysis and condensation reaction of alkoxysilane precursors such as PDMOS. The formation of silanols species results in a shift from a hydrophobic to a hydrophilic environment, thus triggering the block copolymer self-assembly into a lyotropic phase. The ordered mesophases are eventually fixed through the formation of a solid silica network around the mesophases. After irradiation, all the resultant P123-silica films were dry and optically transparent. Film thickness was assessed before and after irradiation by associating the adsorbance value obtained via Fourier-transform infrared spectroscopy with a direct thickness measurement optained via an optical profilometer (Altisurf 500). They were scratched from the substrate and analyzed without any further treatment.

2.3 Characterization

^{1}H and ^{13}C solid-state NMR. ^{1}H magic angle spinning (MAS) NMR, ^{13}C Magic Angle spinning spectra with high-power proton decoupling (MAS+DEC) and ^{1}H-^{13}C heteronuclear correlation (HETCOR) NMR spectra of hybrid materials were recorded on a Bruker AVANCE II 400WB spectrometer (B_0 = 9.4 T) operating at 400.18 MHz for the ^{1}H and 100.64 MHz for the ^{13}C nucleus. ^{1}H MAS NMR experiments were performed with a 2.5 mm double resonance MAS probe at a speed of 30 kHz, with a proton $\pi/2$ pulse duration of 2 μs, a recycle delay of 5 s. ^{1}H spin-lattice relaxation times (T_1) were measured with the inversion-recovery pulse sequence for all samples. Typically, 128 scans were recorded. ^{13}C MAS+DEC and ^{1}H-^{13}C HETCOR NMR experiment were performed with a 4 mm double resonance MAS probe at a speed of 12 kHz and 14 kHz respectively. ^{13}C MAS+DEC NMR spectra were recorded with a $\pi/2$ pulse duration of 2.6 μs, a recycle delay of 60 s and a high-power proton decoupling of 41 kHz during the acquisition. ^{1}H-^{13}C HETCOR NMR experiments were performed using a ramp for Hartmann-Hahn matching with the spinning frequency, with a ^{1}H $\pi/2$ pulse duration of 5.3 μs, a contact time of 1 ms, a recycle delay of 1 s. ^{29}Si MAS+DEC NMR spectra were recorded on a Bruker AVANCE II 300WB spectrometer (B_0 = 7.0 T) operating at 300.07 MHz for the ^{1}H and 59.61 MHz for the ^{29}Si, with a 7 mm double resonance MAS probe at a speed of 4 kHz, a $\pi/6$ pulse duration of 2 μs, a recycle delay of 80 s and a high-power proton decoupling of 59 kHz during the acquisition. Typically, 800 scans were recorded. All the NMR experiments were performed at room temperature. Chemical shifts were referenced to tetramethylsilane. Assignment of NMR resonances was performed with Topspin 3.1 software. The deconvolution of the experimental ^{1}H MAS NMR spectra was performed with DMFIT 2015 Software, a well-established tool designed for fitting NMR spectra, including solid state NMR software [24]. Excellent fittings were achieved when resonances were simulated with the same value of Gaussian (G) /lorentzian (L) parameter $(x \times G)/(1 - x \times L) = 0$, corresponding to Lorentzian resonance type). The full width at half

maximum (FWHM) is given by the distance between points on the curve at which the function reaches half its maximum value.

^1H NMR relaxation experiments. They were performed in a 10 mm NMR tube on a Bruker Minispec MQ-20 spectrometer operating at a proton resonance frequency of 20 MHz with a permanent magnet of B_0 = 0.47 T. The length of the 90° pulse, the dead time of the receiver and the dwell time were 3.44 μs, 9.2 μs and 0.7 μs, respectively. The experiments were performed at 45 °C (initial magnet temperature) under static conditions. Before analysis, the proton spin–lattice relaxation times T_1 were measured for all samples using the inversion-recovery pulse sequence in order to determine and optimize the recycle delay. A range 40 - 60 ms in T_1 was found for all samples and a common recycle delay of 1 s was used. The Free Induction Decay (FID) was recorded by using the simplest pulse sequence:

$$\left(\frac{\pi}{2}\right) - acquisition$$

FID is the simplest NMR sequence and its intensity is directly proportional to the total amount of protons in the sample. The FID intensity is considered at the first point of the decay curve. This point is recorded currently after the receiver dead time (RDT) of the spectrometer (RDT = 9.2 μs). The intensity is confirmed by the recording of a solid echo with a time echo of 9.5 μs. The proton spin-spin relaxation times (T_2) were measured by the Carr-Purcell-Meibloom-Gill (CPMG) pulse sequence:

$$\left(\frac{\pi}{2}\right)_x - (\tau - \pi_y - \tau - acquisition)_n$$

Where *x* and *y* indicate the radio-frequency phases of the pulses with angles π/2 and π, respectively, and τ is the interpulse spacing. The four-step phase cycle, known as CYCLOPS (CYCLically Ordered Phase Sequence), was used to suppress the quadrature detection imbalances which might weaken the CPMG signal. The interpulse spacing τ was taken at the value of 0.05 ms for all the analyses. A number of echo n = 500 was taken for all analyses.

Other analyses. Film thickness was measured by an optical profilometer (Altisurf 500). The films have a typical thickness of 3 ± 0.2 nm. XRD patterns of the as-prepared and calcined samples were obtained on a X'Pert Pro (PANalytical) diffractometer using Cu Kα radiation (λ = 0.15418 nm; 0.5° < 2θ < 10°; 0.017° s^{-1}). Morphology of the as-synthesized hybrid products was observed by transmission electron microscope (TEM) with a JEOL ARM200F at 200 kV.

3. Results and Discussion

3.1 XRD and TEM analysis of mesoscopic ordering in copolymer-silica hybrid

A range of seven block copolymer-silica hybrid films were synthesized by gradually increasing the concentration of PEO-*b*-PPO-*b*-PEO P123 triblock copolymer (10 – 100 wt%). The synthetic procedure is based on light induced self-assembly. The essential chemistry is the UV decomposition of the diaryl iodonium salt Φ_2I^+ PF_6^- resulting in the photocontrolled generation of H^+ PF_6^- superacid, a recognized sol-gel catalyst. The differences with a conventional process based on evaporation induced self-assembly were commented in separate publications [23,25]. In all instances, a solid transparent film was obtained reflecting the onset of a silica inorganic network. Interestingly, the extent of condensation is high (78 % ± 5 %) as revealed by ^{29}Si MAS+DEC NMR with very little change upon varying the P123 concentration (see the relative fractions of Q^n silica species in the spectra of **Figure 1**). Consequently, the silica matrix can be considered as both rigid and similar in terms of structure for all the analyzed samples.

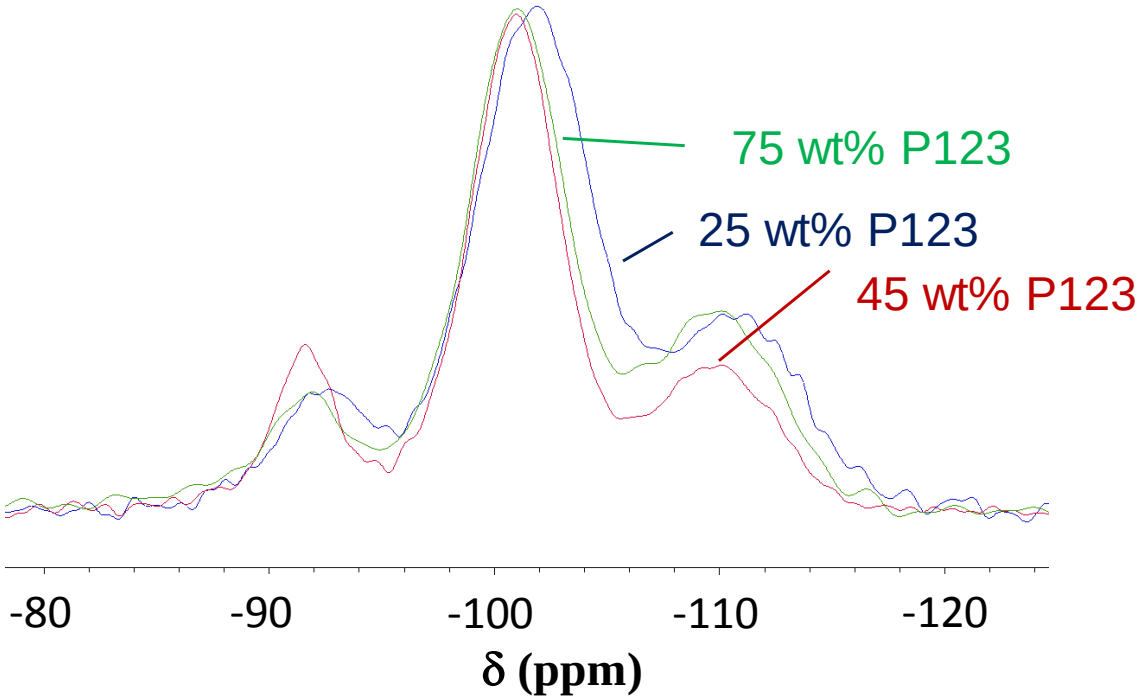

Figure 1. ^{29}Si MAS+DEC NMR spectra of P123 copolymer-silica films prepared with different concentrations of templating agent (25, 45, 75 wt%)

XRD analysis. **Figure 2** shows a series of XRD patterns for five representative composite films (25, 35, 55, 75 and 100 wt% P123). The general trend is that the XRD peaks become more intense and narrow upon increasing the concentration of P123, thus reflecting an increased long-range mesostructuration ordering in the material. At low concentration in templating agent (25 wt%), only a single and weak peak is visible, suggesting a very small proportion of mesostructured domains. At medium P123 concentration (35 – 55 wt%), the XRD pattern shows the (100), (200) and (300) diffraction peaks attributed to a 2D hexagonal mesostructure (*p6mm*). Such assignment (not to be confused with a lamellar mesostructure) is due to the alignment of the hexagonally packed cylinders parallel to the substrate. Such preferential orientation of the 2D hexagonal structure was also supported by grazing-incidence small-angle X-ray scattering measurements (see data in ref. [21]). Fractions of block copolymers higher than 75 wt% gave rise to a lamellar mesostructural ordering. The XRD pattern indicated in this regime a *d-spacing* of 85 - 86 Å, which is somewhat higher than

the *d-spacing* of 75 - 80 Å found in the hexagonal phase (35 – 55 wt%). In addition, calcination at 300 °C was useful to differentiate the two mesostructures: the lamellar phase collapsed, leading to a featureless XRD pattern for the calcined film whereas the reflections of the hexagonal samples were consistently retained (data not given).

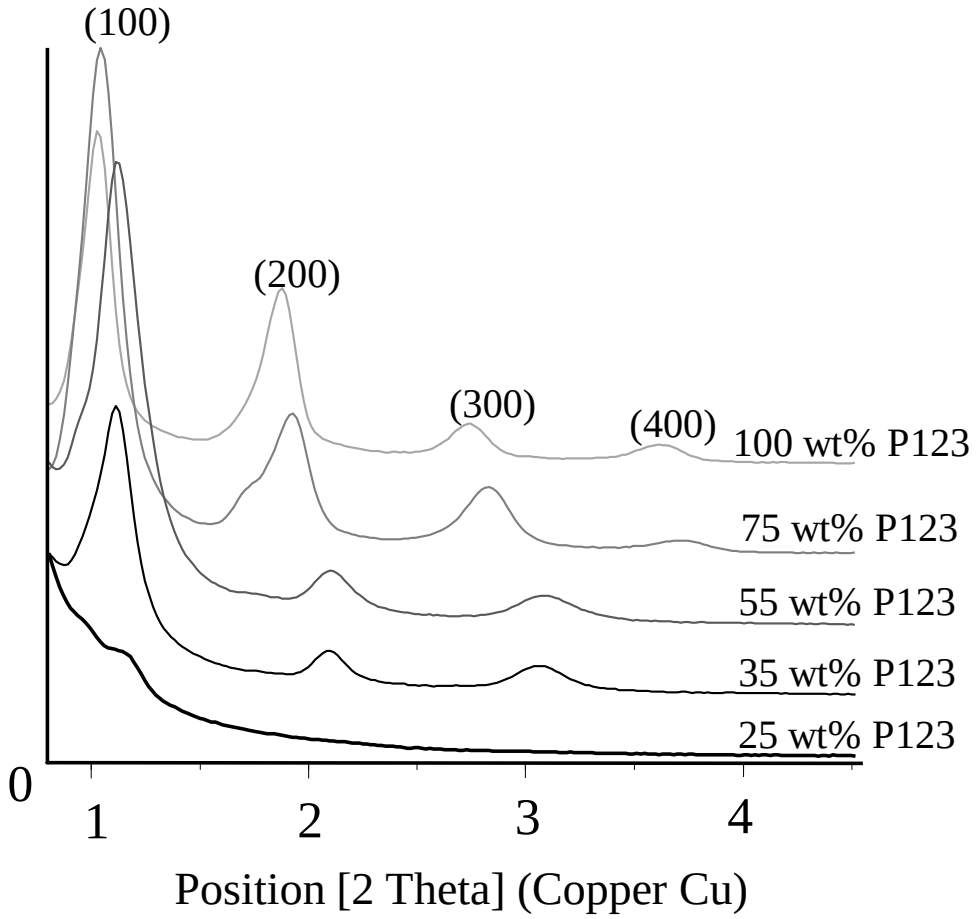

Figure 2. XRD patterns of P123/silica films prepared with different concentrations of amphiphilic block copolymer: 25, 35, 55, 75 and 100 wt%.

TEM analysis. Additionally, TEM images of the as-synthesized P123-silica film samples confirmed that mesostructural ordering is strongly correlated with the concentration of P123. In **Figure 3**, TEM image **a** of the 25 wt% copolymer sample revealed a mostly amorphous structure with a minimal amount of mesoscopic features consisting of isolated hexagonal arrays as well as disordered wormlike aggregates. Conversely, mesostructured domains were observed throughout the majority of the sample for the 45 wt%

copolymer/silica sample in the image **b**. In particular, some finger-print like patterns were clearly visible and tentatively assigned to hexagonal mesostructures aligned parallel to the substrate, thus supporting the XRD data. Further increase of the block copolymer content to 75 wt% induced a change of morphology. The TEM image **c** was consistent with a highly ordered lamellar mesostructure. Viewed from the side, the nanolayers revealed a periodicity persisting over large domain sizes (> 0.5 μm^2). Viewed from the top, they appear rather as step-like features with a set of lamellae planes stacked on top of each other. In conclusion, XRD and TEM data both support that copolymer-silica hybrid samples can be deemed mostly amorphous for P123 concentrations ≤ 25 wt%, highly ordered for concentrations ≥ 55 wt%, and partially organized between these two values.

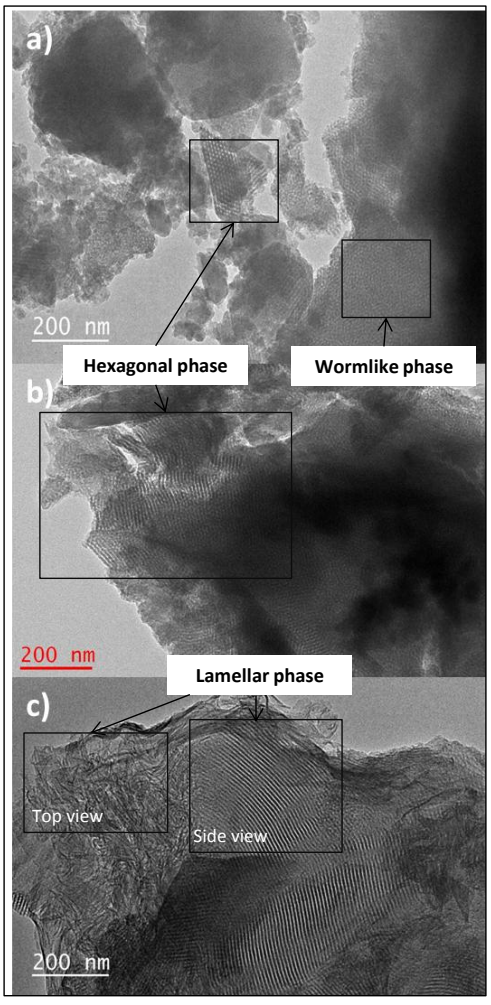

Figure 3. TEM images of a 25 wt% P123-silica film showing poorly ordered aggregates (**a**); 45 wt% P123-silica film displaying hexagonal and wormlike structures forming the larger part of the sample (**b**); and 75 wt% P123-silica film formed by the stacking of lamellar mesophases (**c**).

3.2 ^{1}H and ^{13}C MAS NMR analysis of mesoscopic ordering in copolymer-silica hybrid

3.2.1 Assessment of chemical environment uniformity: ^{13}C MAS+DEC NMR

Figure 4 shows the MAS+DEC ^{13}C spectra of three representative composite films (25, 45 and 75 wt% P123). In the inset, the 45 wt. % P123-silica sample was deconvoluted so as to reveal the different carbon assignments. The isolated narrow feature at ~ 18 ppm was easily assigned to the PPO methyl. The carbons from CH_2 (PPO, PEO) and CH (PPO) arise as an envelope located at 65-80 ppm, which can be decomposed into a triplet resonance with a broad resonance centred at 70.6 ppm associated with the PEO methylene group, whereas the two sharp resonances at 75.7 and 73.6 ppm result from the CH and CH_2 of the PPO block, respectively. Our assignment is in agreement with literature data [26]. A dramatic increase in resolution accompanies the increase of copolymer concentration, thus translating the effect of mesostructuration.

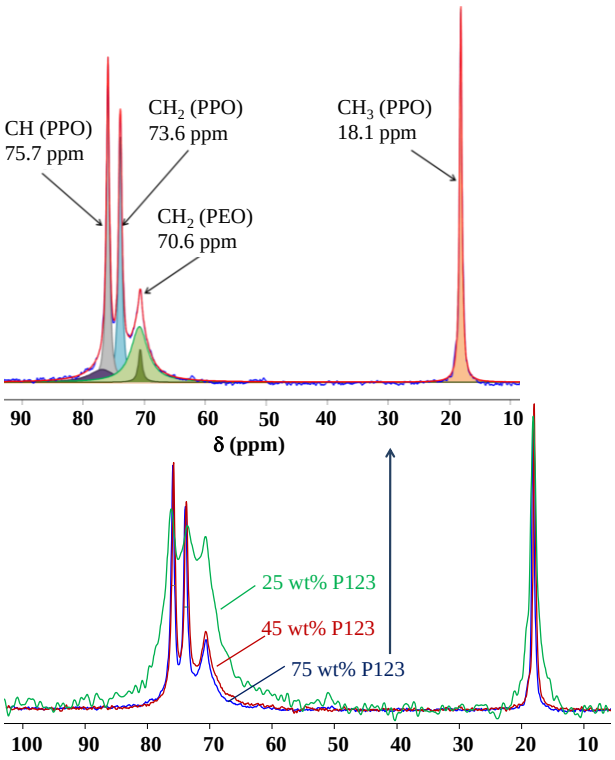

Figure 4. Effect of the concentration of P123 (25, 45 and 75 wt%) on the ^{13}C MAS+DEC NMR spectra of P123-silica film. The inset depicts a deconvoluted spectrum of the hybrid sample containing 75 wt% P123.

In the ^{13}C spectra, the dominant interaction is the isotropic chemical shift of the carbons, since the anisotropic shift as well as the dipolar couplings are generally efficiently suppressed by MAS and dipolar decoupling of DEC analysis. Therefore, the resonance line width is mainly determined by the degree of order of the local environment of the carbon nucleus, explaining that highly ordered samples at 45 % or 75 wt% copolymer show relatively narrow lines. The contrast is obvious with the poorly mesostructured 25 wt% P123/silica composite. In this case, most copolymer blocks are randomly and homogeneously occluded within the silica network, leading to a distribution of isotropic chemical shifts, and therefore broad lines. As a final comment, one can draw an analogy between copolymer self-assembly and polymer crystallization, both resulting in a narrow ^{13}C spectrum. Obviously, densely packed chains in a crystalline phase are much more rigid than copolymer chains in a self-assembled system. However, the chains "feel" a similar chemical environment in both cases, which is eventually the decisive parameter determining the shape of the ^{13}C spectrum.

3.2.2 Assessment of chain mobility: ^{1}H MAS NMR

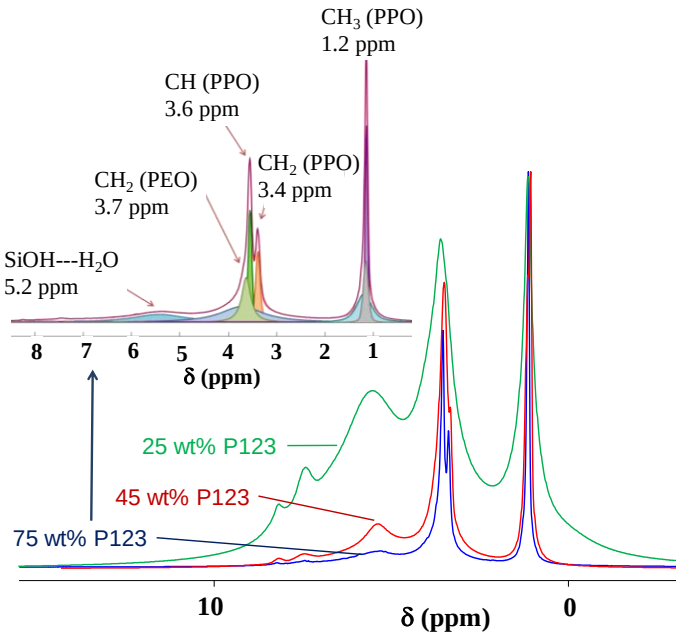

Figure 5. Effect of the concentration of P123 (25, 45 and 75 wt%) on the ^{1}H MAS NMR spectra of P123-silica films. The inset depicts a deconvoluted spectrum of the film prepared with 75 wt% P123.

The ^{1}H MAS NMR spectra of the same three hybrid films (25, 45 and 75 wt% P123) are depicted in **Figure 5**. Speciation in this spectrum is less trivial than the ^{13}C spectrum, and contradictory interpretations were reported in the literature [16,17]. The narrow feature at 1 ppm was straightforwardly attributed to the PPO methyl protons, but some difficulties arise for the massif spanning 2-4 ppm including the unresolved contributions from the CH and CH_2 protons. In this region, valuable information was obtained from ^{13}C-^{1}H heteronuclear correlation (HETCOR) experiments (see **Figure 6** for the 45 wt% P123 sample), based on cross polarization through dipolar coupling. Clearly, the ^{13}C resonances located at 73.6 (CH_2^{PPO}), 75.7 (CH^{PPO}) and 70.6 (CH_2^{PEO}) ppm were correlated to three distinct ^{1}H resonances located at 3.4, 3.6 and 3.7 ppm, thus allowing their attribution. These results confirm the interest of 2D heteronuclear experiments for the characterization of unresolved array of ^{1}H resonances. Finally, the broad downfield resonance at ~ 5 ppm could be assigned to residual silanol protons involved in a variety of H-bonds (water, PEO, PPO).

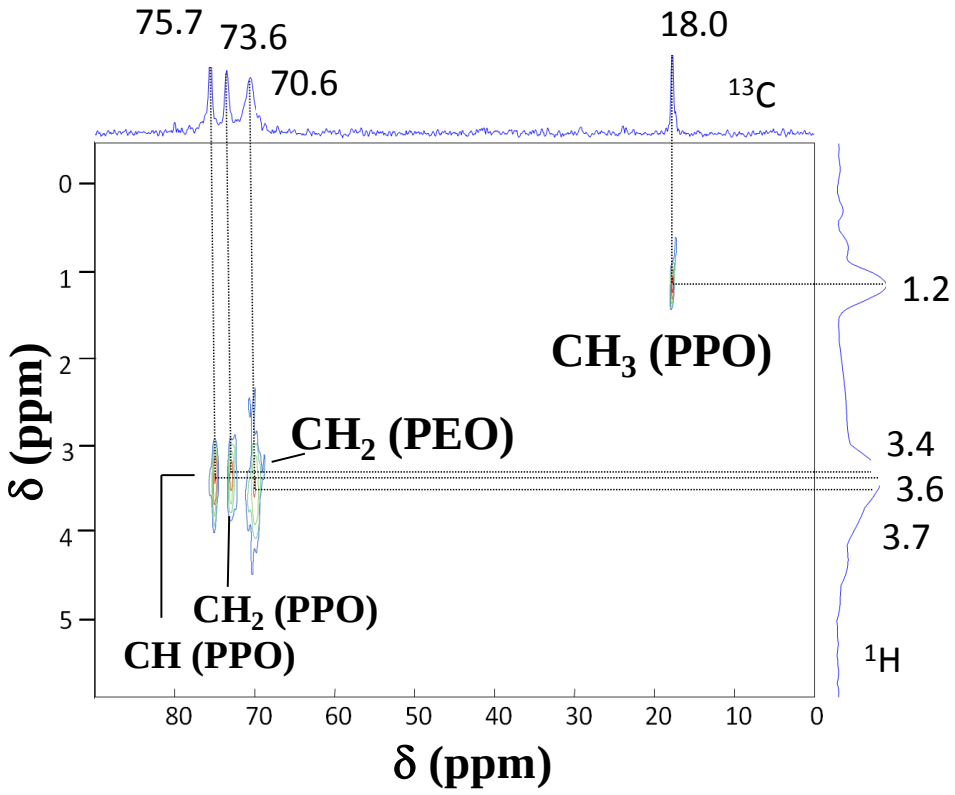

Figure 6. 2D ^{13}C-^{1}H HETCOR NMR spectrum of the 45 wt. % P123-silica hybrid film. ^{13}C and ^{1}H spectra are plotted along their respective axes.

We observe again a significant line narrowing as the copolymer content increases, reflecting the effect of self-assembly. However, the origin of line narrowing is different in ^{1}H and ^{13}C spectra. In ^{1}H spectra, the dominant interaction is rather the strength of the dipolar coupling among the proton nuclei involved, which is very sensitive to motional processes within the material. In the highly ordered mesostructures (50 and 75 wt%), the interfacial surface between the antagonist blocks is significantly reduced, resulting in a greater mobility. Consequently, effective block segregation is manifested by a substantial sharpening of the resonances since the ^{1}H-^{1}H dipolar interactions are averaged out by faster molecular motions. In contrast, the mostly amorphous hybrid microstructure (25 wt% P123) in which the rigid silica network is intimately and randomly mixed with the copolymer experience increased dipolar interactions, yielding a significant line broadening.

3.2.3 ^{1}H and ^{13}C line widths as marker of self-assembly

Whether in the ^{13}C or in the ^{1}H spectrum, line narrowing has been demonstrated as a sensitive marker of the amphiphilic block copolymer self-assembly, although its origin is different in each case. The proton and carbon FWHM were measured for the various PEO-*b*-PPO-*b*-PEO/silica composites, and plotted as function of the templating agent concentration. Regarding the ^{1}H lines in **Figure 7a**, only the three signals from PPO (CH_3, CH and CH_2) were exploited because the deconvolution required in this case a single peak to obtain a good fitting (see inset of **Figure 5**). By contrast, the CH_2^{PEO} feature at 3.7 ppm was discarded because it required a complex treatment with at least one thin and broad component. As expected, all the PPO protons experienced a substantial narrowing upon increasing the content of P123. For example, from 25 to 75 wt% block copolymer, the CH_3 species at 1.25 ppm sharpened considerably, as evident from the FWHM values decreasing from 482 Hz to 55 Hz, a final value very close to that of neat P123 (40 Hz). This result is thus consistent with

a displacement of the PPO block from the rigid silica matrix to the more mobile interior of the mesophase. In addition, a threshold concentration for the mesophase formation can be roughly estimated, between 40 -50 wt% P123. Above this value, the line widths had hardly changed. **Figure 7a** shows, however, lower values at 45 % (hexagonal) compared to 75 % (lamellar), suggesting that copolymer motions might be dependent on mesostructure type. Nevertheless, it is difficult to draw general conclusions because the difference remains small and other parameters can affect FWHM values: slight differences in silica degree of condensation, mixture of mesophases, fraction of ordered domains, etc.

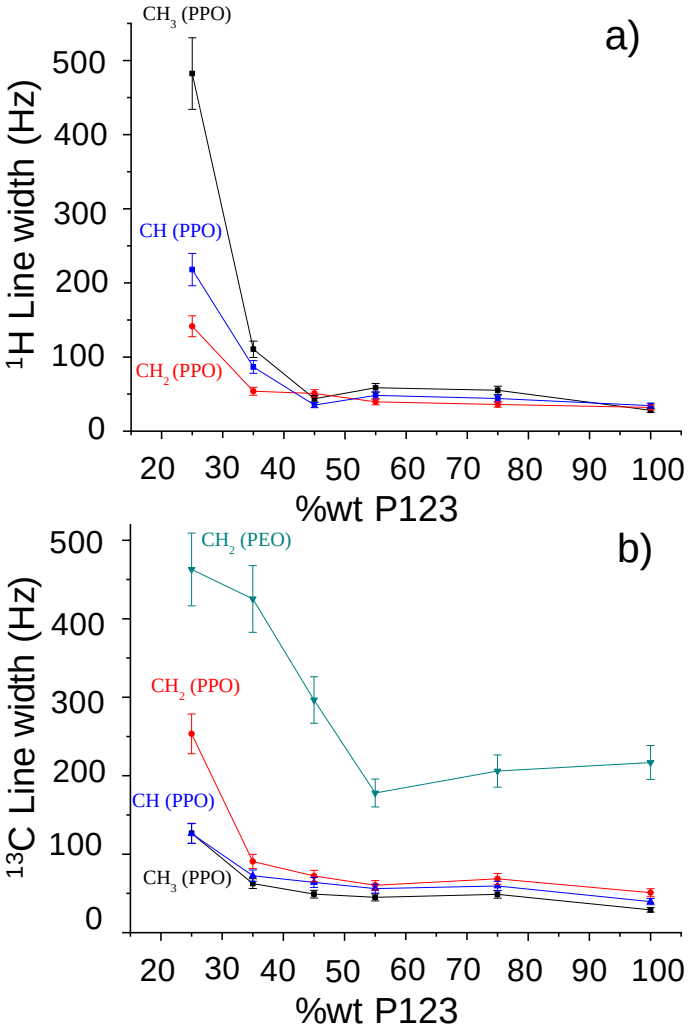

Figure 7. FWHM measurements extracted from the ^{1}H MAS NMR spectra (**a**) and the ^{13}C MAS+DEC NMR spectra (**b**) as a function of P123 concentration (25 – 100 wt%) in the copolymer/silica films.

More resolved, the ^{13}C NMR spectra allowed measuring unambiguously the FWHMs for all carbons, not only from PPO but also PEO (see inset of **Figure 4**). Except for the 100 wt% P123 sample, the three carbon assigned to PPO (CH_2^{PPO}, CH^{PPO} and CH_3^{PPO}) were all substantially narrower than the CH_2^{PEO} feature. This is in accord with the higher interactions of PEO chains with the silica matrix reducing the mobility even when mesophases are present (> 40 wt% P123). However, as can be seen in **Figure 7b**, line narrowing has involved not only the PPO segments, but also the PEO block. At 75 wt% copolymer, the CH_2^{PEO} appeared to be three times narrower than at 25 wt%. Such results may be perceived as surprising because the PEO segments remain in interactions with the silicate network even when highly ordered mesophases are formed at high P123 content. Although self-assembly does not induce a complete segregation of the PEO segments from the silica matrix, it promotes their concentration at the silica/PPO interface. It is expected that, in this configuration, PEO chains have less contact with the rigid environment, thus improving molecular motion and reducing couplings. Collectively, the ^1H and ^{13}C solid-state NMR results agree with the transition from a homogeneous P123-silica blend to a progressive phase separation of the blocks to form a highly ordered mesostructure.

3.3 ^1H T_2 NMR relaxation measurements to study mesoscopic ordering in copolymer-silica hybrid

3.3.1 ^1H T_2 relaxation experiments

The principle is to study the relaxation of a set of magnetic spins placed in a static magnetic flux $\overrightarrow{B_0}$ (parallel to z) and subjected to short pulses of a second surimposed electromagnetic flux $\overrightarrow{B_1}$ in the (x, y) plane (i.e perpendicular to $\overrightarrow{B_0}$). When $\overrightarrow{B_1}$ is turned off, the component of the magnetization in the (x, y) plane M_{xy} starts decreasing. The envelope of this impulse response function M_{xy} is known as the *transverse relaxation function* [27]. For

simple cases of relaxation measurements, its decay is exponential with a time constant T_2, known as the *transverse relaxation time* because the nuclei (essentially ^{1}H) start exchanging energy with each other after the magnetic pulse is stopped. As the excited nuclear spins return to thermal equilibrium, the rates at which ^{1}H spins relax depend on the dipolar coupling strength between the protons, which are strong functions of species mobility. In a nutshell, protons restricted in motion will display a much faster relaxation compared to more mobile protons. Consequently, the high sensitivity of T_2 relaxation to protons dynamics makes this technique potentially useful to assess the disorder-to-order transition in copolymer/silica films. Originally utilized as a means to assess the environment of water in food products [22], T_2 relaxation experiments have expanded to include polymers [28], in order to investigate particle-elastomer interactions in (nano)composite materials [29], semi-crystalline polymers' morphology and dynamics [30] and polymer network [31,32]. In our study, protons content in the seven copolymer/silica samples was evaluated by studying the free induction decay (FID) signal obtained once the 90° $\overrightarrow{B_1}$ pulse is turned off. Because of the high condensation degree of the silica network, the P123 was found as the main source of protons with a minimal content of 85 % in the 10 wt% copolymer-silica composite. An average value of 90 ± 5 % was measured with all the seven samples. The remaining protons come from non-condensed silanols (Si-OH), adsorbed water and various aromatic photoproducts resulting from the photoacid generator.

3.3.2 ^{1}H T_2 NMR relaxation to probe copolymer chain mobility

^{1}H T_2 relaxation decay was measured with a standard Carr-Pucell-Meiboom-Gill (CPMG) pulse sequence. In contrast to FID, this well-established sequence eliminates magnetic field and chemical shift inhomogeneities effect, and is also able to accurately measure the relaxation times. **Figure 8** shows the decay of the transverse magnetization signal

for a poorly mesostructured sample containing 10 wt% P123 (empty circles) and a highly ordered composite prepared at 45 wt% P123 (full circles). As expected, the difference of proton signal intensity decays between the two samples reflects the difference in mobility-dependent dipolar interactions. A slower decay for the 45 wt% P123/silica composite translates a higher fraction of phase separation of the PPO and PEO blocks leading to more mobile polymer segments. However, one must bear in mind that the CPMG sequence records only the more mobile protons, while the more rigid fraction corresponding to immobilized polymer response (with a relaxation time < 0.1 ms) is not detectable. Although this characteristic can be regarded as a drawback because only a part of the protons are "seen", the fraction of CPMG signal over the FID signal (detecting all the protons) was here advantageously used to assess the evolution of the mobile fraction between the different composite samples. The CPMG response is assumed to be mainly an "image" of the copolymer dynamics since P123 is the main source of protons and the residual protons (≈ 10 %, e.g. silanol) are likely to be occluded in the silica matrix preventing their detection by this method.

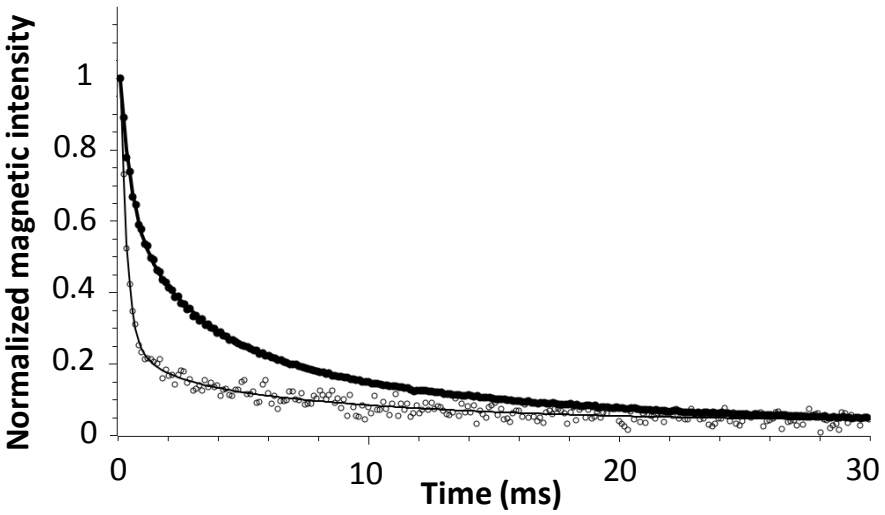

Figure 8. Decay of the transverse magnetization (points are experimental data) for two P123-silica composites having different concentration in P123: at 10 wt% (empty circle) a poorly ordered sample was formed versus a highly ordered sample at 45 wt%, (full circle). The solid lines represent the result of a fitting based on a linear combination of three exponential functions.

Figure 9 is a plot of the protons fraction detected by CPMG as a function of P123 concentration. From a low value of 37 % measured at 10 wt% and 25 wt% P123, the content reached 61 % at 45 wt% P123 (hexagonal), and peaked at 66 % at 75 wt% P123 (lamellar), meaning that 30-35 % of the most rigid protons remain non detectable even in highly ordered samples. Such variation is consistent with an increasing nanophase separation, and the well-defined jump in the 30-40 wt% regime seems indicative of the disorder-to-order transition in the copolymer/silica composites. For mesoscopically ordered samples (≥ 45 wt% P123), the non detected CPMG signal approaches ca. 35 %, a value very close to PEO proton content in P123. This result would suggest that the CPMG signal may be mainly a marker of the segregated protons from PPO hydrophobic block.

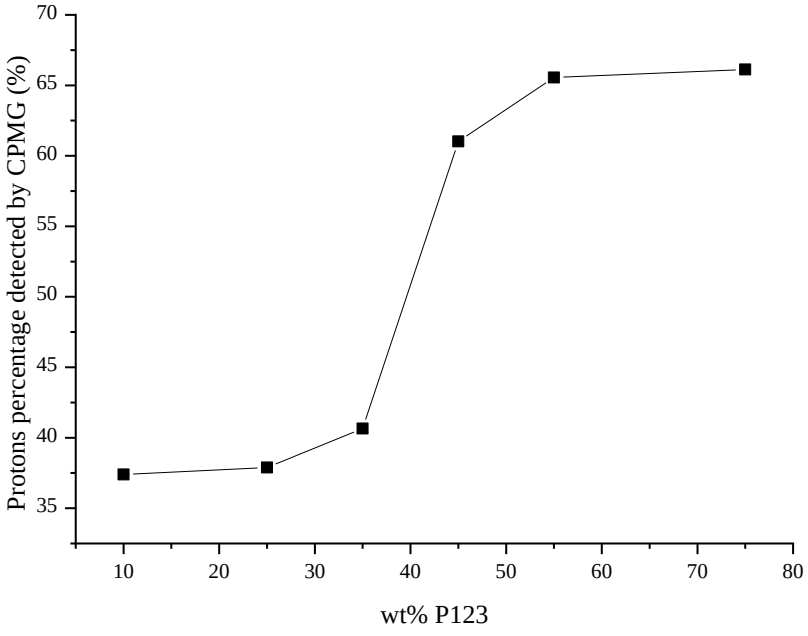

Figure 9. Percentage of protons detected by the CPMG pulse sequence for the copolymer-silica composites containing different concentrations of template (P123).

4 Conclusion

By varying the concentration in templating agent (P123), a series of amphiphilic copolymer-silica composite thin films with different degrees of mesoscopic order were synthesized. Firstly, conventional structural characterization methods based on XRD and

TEM established that highly ordered mesophases could be observed for a threshold concentration of 40-50 wt% in templating agent. By using carbon and proton monodimensional NMR experiments, line narrowing has been correlated with the higher mesoscopic order. The result can be understood on the basis of a higher *chemical uniformity* (^{13}C) and *mobility* (^{1}H) when the copolymer segments phase separate in the course of the self-assembly process. A third means to check the level of ordering of the P123/silica samples was proposed based on ^{1}H transverse relaxation time measured by low-field NMR spectroscopy. The increased fraction of mobile protons from the copolymers segments accompanying mesostructuration can be visualized using the CPMG method. In our study, T_2 relaxometry has proved relevant to detect the disorder-to-order transition that arises above a threshold template concentration of approx. 40 wt%.

Acknowledgements

This work was supported by the Fondation de l'Ecole Nationale Supérieure de Chimie de Mulhouse (France) which has granted a 3-year PhD scholarship to Mrs. Mathilde Sibeaud. We thank P. A. Albouy of the Laboratoire de Physique des Solides (CNRS, UMR8502, Université Paris-Sud, Orsay, France) for performing GISAXS experiments.

References

[1] D. Zhao, Y. Wan, W. Zhou, Ordered Mesoporous Materials, Wiley-VCH, Weinheim, 2013. https://doi.org/10.1002/9783527647866.ch4

[2] S.L. Suib, A Review of Recent Developments of Mesoporous Materials, Chem. Rec. 17 (2017) 1169–1183. https://doi.org/10.1002/tcr.201700025.

[3] W. Li, J. Liu, D. Zhao, Mesoporous materials for energy conversion and storage devices, Nat. Rev. Mater. 1 (2016) 16023. https://doi.org/10.1038/natrevmats.2016.23.

[4] W. Peng, S. Xu, L. Li, C. Zhang, S. Zheng, Organic–Inorganic Nanocomposites via Self-Assembly of an Amphiphilic Triblock Copolymer Bearing a Poly(butadiene-g-POSS) Subchain in Epoxy Thermosets: Morphologies, Surface Hydrophobicity, and Dielectric Properties, J. Phys. Chem. B. 120 (2016)12003-12014 https://doi.org/10.1021/acs.jpcb.6b08026.

[5] V.S.D. Voet, K. Kumar, G. Ten Brinke, K. Loos, Bioinspired Synthesis of Well- Ordered Layered Organic–Inorganic Nanohybrids: Mimicking the Natural Processing of Nacre by

Mineralization of Block Copolymer Templates, Macromol. Rapid Commun. 36 (2015) 1756−1760. https://doi.org/10.1002/marc.201500301.
[6] M. Stefik, S. Guldin, S. Vignolini, U. Wiesner, U. Steiner, Block copolymer self-assembly for nanophotonics, Chem. Soc. Rev. 44 (2015) 5076–5091. https://doi.org/10.1039/C4CS00517A.
[7] T.N. Hoheisel, K. Hurr, U. Wiesner, Block copolymer-nanoparticle hybrid self-assembly, Prog. Polym. Sci. 40 (2015) 3–32. https://doi.org/10.1016/j.progpolymsci.2014.10.002.
[8] C. Sanchez, P. Belleville, M. Popall, L. Nicole, Applications of Advanced Hybrid Organic-Inorganic Nanomaterials: from Laboratory to Market, Chem. Soc. Rev. 40 (2011) 696–753. https://doi.org/10.1039/C0CS00136H
[9] M. Faustini, L. Nicole, E. Ruiz-Hitzky, C. Sanchez, History of Organic–Inorganic Hybrid Materials: Prehistory, Art, Science, and Advanced Applications, Adv. Funct. Mater. 28 (2018) 1704158. https://doi.org/10.1002/adfm.201704158.
[10] G.K. Sethi, X. Jiang, R. Chakraborty, W.S. Loo, I. Villaluenga, N.P. Balsara, Anomalous Self-Assembly and Ion Transport in Nanostructured Organic–Inorganic Solid Electrolytes, ACS Macro Lett. 7 (2018) 1056–1061. https://doi.org/10.1021/acsmacrolett.8b00583.
[11] C. Boissiere, D. Grosso, S. Lepoutre, L. Nicole, A.B. Bruneau, C. Sanchez, Porosity and mechanical properties of mesoporous thin films assessed by environmental ellipsometric porosimetry, Langmuir. 21 (2005) 12362–12371. https://doi.org/10.1021/la050981z.
[12] M.R. Landry, Thermoporometry by differential scanning calorimetry: experimental considerations and applications, Thermochim. Acta. 433 (2005) 27–50. https://doi.org/10.1016/j.tca.2005.02.015.
[13] M.P. Petkov, M.H. Weber, K.G. Lynn, K.P. Rodbell, Porosity characterization by beam-based three-photon positron annihilation spectroscopy, Appl. Phys. Lett. 79 (2001) 3884–3886. https://doi.org/10.1063/1.1421090.
[14] R. Kennard, W.J. DeSisto, T.P. Giririjan, M.D. Mason, Intrinsic property measurement of surfactant-templated mesoporous silica films using time-resolved single-molecule imaging, J. Chem. Phys. 128 (2008) 128, 134710. https://doi.org/10.1063/1.2868751.
[15] C. Bonhomme, C. Gervais, D. Laurencin, Recent NMR developments applied to organic-inorganic materials, Prog. Nucl. Magn. Reson. Spectrosc. 77 (2014) 1–48. https://doi.org/10.1016/j.pnmrs.2013.10.001.
[16] N.A. Melosh, P. Lipic, F.S. Bates, F. Wudl, G.D. Stucky, G.H. Fredrickson, B.F. Chmelka, Molecular and Mesoscopic Structures of Transparent Block Copolymer-Silica Monoliths, Macromolecules. 32 (1999) 4332–4342. https://doi.org/10.1021/ma9817323.
[17] B. Alonso, T. Mineva, P. Innocenzi, G. Trimmel, K. Stubenrauch, I. Melnyk, Y. Zub, F. Fayon, P. Florian, D. Massiot, Perspectives in 1H, 14N and 81Br Solid-State NMR Studies of Interfaces in Materials Textured by Self-Assembled Amphiphiles, CR Chim. 13 (2010) 431–442. https://doi.org/10.1016/j.crci.2009.
[18] B. Alonso, C. Marichal, Solid-state NMR studies of micelle-templated mesoporous solids, Chem. Soc. Rev. 42 (2013) 3808–3820. https://doi.org/10.1039/c2cs35368g.
[19] B. Alonso, C. Bonhomme, C. Gervais, F. Guenneau, D. Laurencin, F. Ribot, Nuclear Magnetic Resonance as a Tool for the Investigation of Interfaces and Textures, in: M- H. Delville, A. Taubert (Eds.), Nanostructured Hybrid Materials: Hybrid Organic- Inorganic Interfaces, John Wiley, Weinheim, 2017: pp. 839–865. https://doi.org/10.1002/9783527807130.ch20.
[20] B. Alonso, F. Fayon, D. Massiot, H. Amenitsch, L. Malfatti, T. Kidchob, S. Costacurta, P. Innocenzi, Hybrid Organic-Inorganic Mesostructured Membranes: Interfaces and Organization at Different Length Scales, J. Phys. Chem. C. 114 (2010) 11730–11740. https://doi.org/10.1021/jp101652a.
[21] M. Sibeaud, H. De Paz-Simon, C. Croutxe-Barghorn, S. Rigolet, L. Michelin, B. Lebeau, L. Vidal, P.-A. Albouy, A. Chemtob, Scaling-up of mesoporous silica films via an eco-efficient UV processing method. Part 1: Photoinduced mesostructuration, Microporous Mesoporous Mater. 257 (2018) 42–50. https://doi.org/10.1016/j.micromeso.2017.08.017.
[22] J. Mitchell, L.F. Gladden, T.C. Chandrasekera, E.J. Fordham, Low-field permanent magnets for industrial process and quality control, Prog. Nucl. Magn. Reson. Spectrosc. 76 (2014) 1–60. https://doi.org/10.1016/j.pnmrs.2013.09.001.

[23] H. De Paz-Simon, A. Chemtob, C. Croutxe-Barghorn, S. Rigolet, L. Michelin, L. Vidal, B. Lebeau, Periodic Mesostructured Silica Films Made Simple Using UV Light, J. Phys. Chem. C. 118 (2014) 4959–4966. https://doi.org/10.1021/jp410518k.
[24] D. Massiot, F. Fayon, M. Capron, I. King, S. Le Calve, B. Alonso, J.-O. Durand, B. Bujoli, Z. Gan, G. Hoatson, Modeling One- and Two-Dimensional Solid-State NMR Spectra, Magn. Reson. Chem. 40 (2002) 70–76. https://doi.org/10.1002/mrc.984.
[25] H. De Paz, A. Chemtob, C. Croutxé-Barghorn, S. Rigolet, B. Lebeau, A Solvent-Free Photochemical Route for the Preparation of Mesoporous Inorganic Films, Microporous Mesoporous Mater. 151 (2012) 88–92. https://doi.org/10.1016/j.micromeso.2011.10.045.
[26] B. Dragoi, G. Laurent, S. Casale, T. Benamor, B. Lebeau, C. Boissière, F. Ribot, M. Selmane, P. Schmidt, D. Kreher, A. Davidson, Stability and degradation of PEO20PPO70PEO20 triblock copolymers in mesostructured silica, J. Sol-Gel Sci. Technol. 91 (2019) 552–566. https://doi.org/10.1007/s10971-019-05044-w.
[27] B. Blumich, F. Casanova, S. Appelt, NMR at low magnetic fields, Chem. Phys. Lett. 477 (2009) 231–240. https://doi.org/10.1016/j.cplett.2009.06.096.
[28] A. Adams, Analysis of solid technical polymers by compact NMR, Trends Anal. Chem. 83 (2016) 107–119. https://doi.org/10.1016/j.trac.2016.04.003.
[29] A. Papon, K. Saalwachter, K. Schaler, L. Guy, F. Lequeux, H. Montes, Low-Field NMR Investigations of Nanocomposites: Polymer Dynamics and Network Effects, Macromolecules. 44 (2011) 913–922. https://doi.org/10.1021/ma102486x.
[30] L.L. Zhang, E.W. Hansen, I. Helland, E. Hinrichsen, A. Larsen, J. Roots, Crystallinity in Ethene-1-Hexene Copolymers Determined by H-1 and C-13 NMR. A Comparative Study, Macromolecules. 42 (2009) 5189–5195. https://doi.org/10.1021/ma900249z.
[31] J. Hopfner, G. Guthausen, K. Saalwachter, M. Wilhelm, Network Structure and Inhomogeneities of Model and Commercial Polyelectrolyte Hydrogels as Investigated by Low-Field Proton NMR Techniques, Macromolecules. 47 (2014) 4251–4265. https://doi.org/10.1021/ma500558v.
[32] V.M. Litvinov, A.A. Dias, Analysis of network structure of UV-cured acrylates by H-1 NMR relaxation, C-13 NMR spectroscopy, and dynamic mechanical experiments, Macromolecules. 34 (2001) 4051–4060. https://doi.org/10.1021/ma010066u.